




Exceptional strain strengthening and tuning of mechanical properties of TiNChang Liu ^{1,2,3,*}, Xinxin Gao ^{1,2,*}, Kan Zhang ^{1,2,†}, Weitao Zheng,² and Changfeng Chen⁴¹State Key Lab of Superhard Materials, Jilin University, Changchun 130012, China²Key Laboratory of Automobile Materials MOE, and Department of Materials Science, Jilin University, Changchun 130012, China³International Center for Computational Method and Software, College of Physics, Jilin University, Changchun 130012, China⁴Department of Physics and Astronomy, University of Nevada, Las Vegas, Nevada 89154, USA

(Received 14 June 2022; revised 11 August 2022; accepted 22 August 2022; published 29 August 2022)

Transition-metal light-element (TMLE) compounds possess high mechanical strength and hardness desirable for wide-ranging applications; but these materials tend to suffer large loss of shear strength in the presence of a compressive stress normal to the shear plane, which greatly impairs structural integrity and hinders mechanical performances under many practical loading conditions. There is pressing need to explore stress-strain relations to set benchmarks and find mechanisms for property optimization among this broad class of materials. Here, we show by first-principles calculations that titanium nitride (TiN) exhibits strain-induced stress enhancement and homogeneity, rendering enhanced and more isotropic stress responses under diverse compression constrained shear deformation; TiN also exhibits contrasting ductile/brittle stress responses under indentation and wear strains with distinct normal-to-shear stress ratios. Moreover, we assess crystal-orientation dependent strengths to account for experimentally observed directional variations of hardness. Analysis of bonding evolution unveils intricate atomistic mechanisms that dictate the deformation modes and resulting stress responses under various practical loading conditions. Such exceptional strain strengthening and tuning of major mechanical properties makes TiN an exemplary case among TMLE compounds for elucidating strain induced strengthening and load-sensitive ductile/brittle characteristics. These results provide an accurate description and in-depth understanding of diverse calculated and measured properties of TiN and offer insights for further exploration of versatile loading and crystal-orientation dependent mechanical properties among the vast class of TMLE compounds. The present findings raise the prospects of rational design and optimization of these prominent materials tailored for wide-ranging experimental implementation and diverse application.

DOI: [10.1103/PhysRevB.106.054112](https://doi.org/10.1103/PhysRevB.106.054112)**I. INTRODUCTION**

Mechanical strength under versatile loading conditions is a key material property for diverse applications ranging from large-scale equipment to nanoscale devices. This property determines structural integrity and durability of materials and sets limits on their ability to sustain tear and wear under a variety of strains such as compression, tensile, shear, indentation, and wear, among others. There are broad interests in many research fields to find materials that possess high strength and hardness to sustain large mechanical loadings and support additional functionalities. Traditional superstrong solids like diamond and cubic boron nitride offer superior mechanical performances in wide-ranging applications [1], but these materials also have considerable drawbacks, especially their stringent and costly high-pressure and high-temperature synthesis and sintering conditions and, in the case of diamond, strong tendency to oxidize at moderately high temperatures and react with ferrous metals, which greatly limit their usage in many scientific and technological areas. Recent years have seen the rise of a distinct class of

strong materials, namely the transition-metal light-element (TMLE) compounds [2–11], which possess low compressibility due to high valence electron count contributed by TM atoms and high overall structural rigidity stemming from the strong covalent or mixed covalent-metallic bonding among the constituent atoms as in TM carbides, borides, and nitrides. These compounds possess high strength and hardness that are lower than the extremely large values for diamond and cubic boron nitride but nevertheless superior to many functional materials widely used in industrial and technological settings. The TMLE compounds also exhibit high thermal stability and are nonreactive to ferrous metals; their synthesis requires much easier conditions compared to those for traditional superhard materials. These favorable properties make TMLE compounds promising for many practical applications. There exists, however, a major weakness for these materials in that they tend to soften significantly under loading conditions that host coexisting shear stresses and compressive stress normal to the shear plane, which are omnipresent in many testing and application settings. This phenomenon presents a pressing need to search among the TMLE compounds for materials that can overcome this major weakness and, more important, to elucidate the underlying mechanisms for guidance to help improve the ability to deliver consistently strong and durable mechanical performance in diverse application environments.

*These authors contributed equally to this work.

†kanzhang@jlu.edu.cn

There have been extensive studies in recent years on the TM borides [9,10,12–17] that exhibit favorable synthesis conditions, rich material configurations and indentation hardness up to 50–60 GPa at very small loads [18,19]. At higher loads, however, these materials experience drastic drops of hardness by as much as 60–80% [20,21]. The characterization of a material's ability to resist large deformation is better described by its load-independent strength or hardness at large strains [22,23], thereby setting limits on the load-bearing ability in practical environments. Most TMLE compounds exhibit such intrinsic load-independent hardness in the 15–30 GPa range, which is considered good but still well below the 40 GPa threshold commonly designated for superhard materials that are desired for many applications that require extreme material strength and hardness to achieve sufficient equipment durability and sustainability under the most demanding application conditions. The observed large strength reductions in these compounds have been attributed to the considerable strain-induced softening due to the charge redistribution and the associated bond breaking at large structural deformations, which are fundamentally rooted in the peculiar quantum nature of the covalent bonding configurations of light elements, especially boron [24–30]. In contrast, indentation strain stiffening, which is uncommon among crystalline solids, has been shown to be able to enhance material hardness in some traditional superhard solids such as diamond and cubic boron nitride [31–34]. The reported experimental and theoretical studies of tungsten nitrides [35,36] raised the prospects of finding similar strengthening among TM nitrides. However, the synthesis of well-crystallized tungsten nitrides under high-pressure and high-temperature conditions has been extremely challenging and hitherto remains unattainable, hindering further exploration and a full understanding of the strain strengthening phenomena. It is thus desirable that more in-depth studies are carried out to identify the TMLE compounds that possess broadly enhanced stress responses to versatile strains leading to enhanced mechanical properties.

In this paper, we report on a systematic first-principles study of the stress responses and associated structural deformation modes of titanium nitride (TiN) under a large variety and range of pure and normal-stress constrained shear strains. We select TiN for an exemplary case study in this paper because this compound has long been successfully synthesized in bulk and thin-film forms and widely used in applications such as wear-resistant coatings and thus offers a material platform with experimental information to help elucidate the computational results and derive key insights into the underlying atomistic mechanisms. Our calculated stress-strain relations reveal exceptional stress responses of TiN under versatile biaxial compression-shear conditions, producing a series of notably improved mechanical performance benchmarks. First, TiN undergoes broad strengthening under multiple shear deformation modes in the presence of normal stresses that are widely encountered under indentation and wear contact loadings, generating higher peak stresses that set ultimate mechanical strengths, which explains the experimentally measured high hardness. An analysis of the bonding changes in the strengthening process uncovers the atomistic mechanisms for this unusual phenomenon.

Second, calculated stress responses unveil a marked reduction of anisotropic stress responses of TiN under the biaxial stresses. It is well known that the covalent or mixed covalent-metallic bonding networks in TMLE compounds produce directional stress responses with anisotropic deformation patterns. When a significant normal stress is present, stresses along major shear slip directions of TiN become nearly isotropic, driven by bonding variations under the biaxial loading strains compared to those under pure shear strains. Third, the calculated shear stresses are sensitive to loading conditions with different normal-to-shear relations, showing contrasting brittle and ductile behaviors under distinct indentation and wear strains. These findings have implications for mechanical performances under distinct hardness testing and hard-coating application scenarios, raising cautions in using the hardness testing results to interpret and predict mechanical behaviors in loading environments with different normal-to-shear ratios. Fourth, it is noted that stress responses are highly dependent on crystallographic planes on which indentation or wear loads are applied, indicating a clear crystal-orientation dependence of mechanical properties, which is consistent with the experimentally measured indentation hardness results on distinctly oriented TiN and highlight the directional nature of stress-strain relations for TMLE compounds. This study introduces a systematic description of loading and crystal-orientation dependent mechanical properties under diverse strain conditions, and offers insights for effective tuning of structure-property relations toward rational material design and optimization.

The stress-strain relations from first-principles calculations reported here reveal a rich variety of exceptional strain tuning of the mechanical properties of TiN; the results showcase the performance characteristics and elucidate the relations among the various mechanisms connecting and contrasting the distinct mechanical processes that produce different stress responses. The key features of the strain induced structural and bonding changes not only elucidate the mechanical properties of TiN, but also are applicable to other transition-metal nitrides, carbides, and borides that share the fundamental TM-LE bonding characteristics. The insights derived from the present results offer useful guiding principles for further search and study of the mechanical behaviors among the large family of TMLE compounds with broad implications for optimization of their structural and mechanical performances, holding broad promises for precise and tailored material design and discovery for development and implementation in wide-ranging applications.

II. COMPUTATIONAL METHODS

The stress-strain relations obtained from first-principles calculations provide an accurate description of material deformations and mechanical strengths under versatile loading conditions [37–50], and the calculated indentation strengths can be compared directly to the experimental results of nanoindentation measurements [51–53]. Under the large indentation or wear loading conditions, shear instability usually precedes the initiation of cracks and dislocations [54], signaling the onset of incipient plasticity [41,43], and bond collapse may occur under a coexisting compressive stress

[55,56]. Determination of the indentation strength is achieved by the calculations under a biaxial stress field that contains concurrent shear (σ_{zx}) and normal compressive (σ_{zz}) stress components that obey the relation $\sigma_{zx} = \sigma_{zz} \tan \theta$, where θ is the centerline-to-face angle of the indenter [55,56]. We have employed this approach to the study of many TMLE compounds and have found that indentation strengths consistently describe well the measured load-invariant indentation hardness results [24–29]. In this paper, we report the calculated results for TiN under the Vickers indentation with $\theta = 68^\circ$, Berkovich indentation with $\theta = 65.3^\circ$, and the case of $\theta = 0^\circ$ that describes the flat contact geometry commonly encountered during the wear and friction motion when a normal stress is present and covers the pure shear loading condition when a normal stress is absent.

For the calculations reported in this paper, we have employed the VASP code [57], adopting the projector augmented wave method [58] and Perdew-Burke-Ernzerhof (PBE) generalized gradient approximation [59]. A cutoff energy of 500 eV for the expansion of the wave function into plane waves and a $15 \times 15 \times 15$ Monkhorst-Pack k-point sampling meshes [60] have been chosen to ensure that all enthalpy calculations are converged to better than 1 meV/atom. The shape of the unit cell is determined by the full atomic relaxation without any imposed boundary conditions with the stress convergence set to 0.1 GPa.

The stress-strain relations have been obtained following a quasistatic loading approach [37,47,55,56] where the lattice vectors were incrementally deformed in the direction of the applied strain. At each step of the structural deformation process, the applied shear strain along the chosen loading path is fixed which determines the calculated stress response, while the other five independent components of the strain tensors and all the atoms inside the unit cell are simultaneously relaxed until (i) the stress normal to the shear slip plane has reached a specified value corresponding to the normal-stress component set by the indenter geometry under the indentation condition or the directly applied normal stress under the sliding contact condition, (ii) all the other residual components of the Hellmann-Feynman stress tensor orthogonal to the applied strain are less than 0.1 GPa, and (iii) the force on each atom becomes negligible. The shape of the unit cell is determined by this constrained atomic relaxation procedure without any imposed boundary conditions.

III. RESULTS AND DISCUSSIONS

The ground-state crystal phase of TiN adopts the NaCl-type cubic structure (space group Fm-3m, No. 225), as shown in Fig. 1(a). Our calculations have produced the lattice parameter $a = 4.255 \text{ \AA}$, which is in good agreement with the experimental value of 4.240 \AA [61]. The calculations were performed at $T = 0 \text{ K}$ and the experiment was done at the room temperature; given that the thermal expansion coefficient of TiN is on the order of 10^{-6} K^{-1} [62], a temperature difference of around 300 K has minimal impact on the comparison of the calculated and measured lattice parameters. The slight overestimate of the calculated lattice parameter compared to the experimental value is a well-known feature of the GGA formalism. To assess

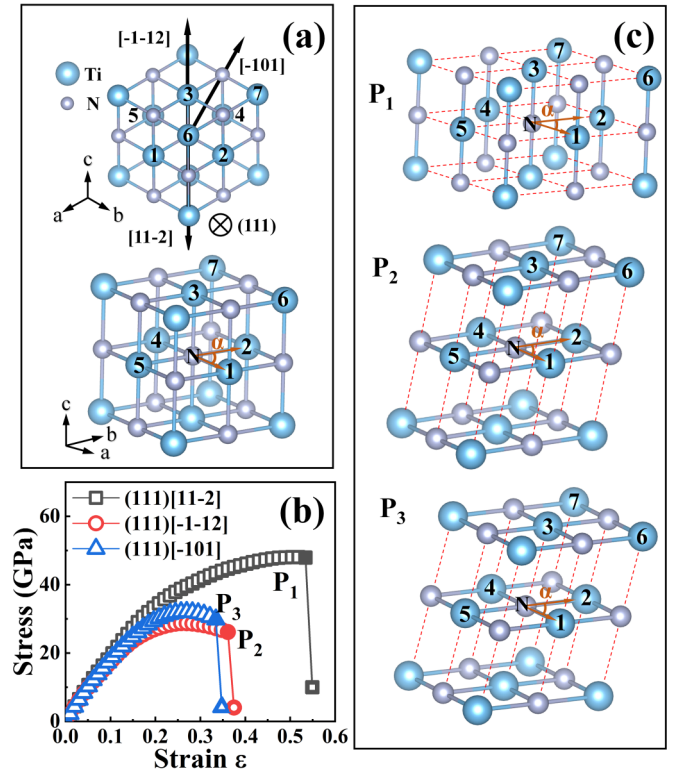


FIG. 1. (a) Crystal structure of TiN at equilibrium in 2D view in the (1 1 1) plane. (b) The calculated stress responses of TiN under the pure shear strains in the (1 1 1) plane along the major high-symmetry [1 1 -2], [-1 -1 2], or [-1 0 1] shear slip directions. (c) The structural snapshots right before the large stress drop. The dashed lines indicate the most stretched main load-bearing N-Ti bonds [see Fig. 2(a) for details].

the mechanical properties under the indentation and flat-contact conditions occurring in the hardness test and wear environments typically encountered in applications, we have systematically examined stress responses under a wide range of shear strains, including the pure shear strains, Vickers and Berkovich indentation shear strains, and constant normal-stress constrained shear strains. We have compared the obtained stress-strain relations under these loading conditions in distinct crystallographic planes to evaluate the dependence of mechanical strength and hardness on crystal orientations. This approach establishes a robust and systematic theoretical framework for describing these prominent mechanical properties on a comprehensive basis and for assessing the associated changes of the bonding patterns to elucidate the atomistic processes and the underlying mechanisms that are crucial to the rational design and optimization of the benchmark performance characteristics. Below we present and analyze the calculated results of structural deformation modes and stress responses of TiN under selected shear strains to establish key material phenomena and unveil the driving mechanisms.

Previous studies have shown [63] that TiN (1 1 1) surface exhibits the highest indentation hardness among the major low-index crystallographic orientations, and the optimal (1 1 1) crystal orientation can be controllably achieved in the

films grown by direct current reactive magnetron sputtering on substrates with applied bias voltages [64–66]. Therefore, we first take the TiN (1 1 1) plane as a primary case study in this section to assess the stress responses under pure shear strains, which is followed in the next two sections by a systematic and in-depth examination of the effects of the distinctive normal compressive stresses introduced by the indentation and wear shear loadings in the TiN (1 1 1) plane. We then compare, analyze, and elucidate the fundamentally interesting and practically impactful phenomenon of load-dependent brittle-ductile variation induced by distinct combinations of normal and shear strains compared to the benchmark results obtained under the corresponding pure shear strains. Finally, we examine stress responses under pure and various constrained shear deformation modes in the other two major low-index (1 1 0) and (0 0 1) planes to make a systematic and comparative analysis of the orientation dependent mechanical properties of TiN, aiming to derive the key insights into the fundamental atomistic mechanisms that are likely to be shared by other TMLE compounds.

A. Structural deformation and stress responses of TiN under pure shear strains

We first investigate the stress responses of TiN under pure shear strains to establish the essential benchmark mechanical characteristics that measure the material's intrinsic ability to resist shape-changing deformations. From the calculated stress-strain relations, the initial stress responses at small strains determine the shear moduli along various shear slip directions that are commonly used to describe pertinent mechanical behaviors; more important, the results over the wide ranges of deformation up to the elastic limits provide further, much richer information on the structural and mechanical properties, especially the bonding changes and corresponding stress variations that offer insights into the atomistic mechanisms driving the stress responses. Moreover, these benchmark properties also provide the crucial reference for well-pointed comparisons with stress response behaviors under a wide variety of more complex shear strains that are relevant to versatile loading conditions in many realistic settings, including the indentation and wear environments that are also systematically examined in this paper.

We present in Fig. 1 the calculated stress responses and associated key structural bonding deformation modes of TiN under the pure shear strains in the (1 1 1) plane along several indicated major high-symmetry slip directions over the whole strain range reaching and past the elastic limits as marked by the steep drop of stress due to the loss of the original bonding configuration in each case. The results in Fig. 1(b) show that the lowest pure shear peak stress occurs in the easy-slip (1 1 1)[$-1 -1 2$] shear direction with a value of 28.7 GPa, and this lower threshold stress determines the ideal pure shear strength of TiN on its (1 1 1) plane. Strikingly, the pure shear stress response to strains in the opposite slip direction (1 1 1)[$1 1 -2$] is much stronger with a steeper rise to the considerably larger peak value of 48.1 GPa. This highly contrasting anisotropic stress distribution is reminiscent of the very large shear stress disparity in diamond where distinct bonding arrangements produce drastically different stress responses in opposite shear

directions [37]. Meanwhile, the stress response under the (1 1 1)[$-1 0 1$] pure shear strains are close to but slightly above the weak results under the (1 1 1)[$-1 -1 2$] deformation mode. It is noted that the [1 1 -2] and [$-1 -1 2$] shear slip directions each have a three-fold rotational symmetry in the (1 1 1) plane, while the [$-1 0 1$] direction has a sixfold rotational symmetry. The stress responses along these high-symmetry directions set the framework for projection and interpolation of the results in the higher-index and lower-symmetry directions.

To elucidate the calculated stress-strain relations, we examine the bond deformation modes [Fig. 1(c)] and associated bond-length and bond-angle variations (Fig. 2) of TiN under the pure shear strains in the (1 1 1) plane. It is noted that under the (1 1 1)[$1 1 -2$] pure shear strains, bond elongation mainly occurs in the (0 0 1) plane accompanied by a large angular deformation (see below); meanwhile, under the (1 1 1)[$-1 -1 2$] and (1 1 1)[$-1 0 1$] pure shear strains, bonds along the [0 0 1] direction undergo the most elongation, leading toward (0 0 1) cleavage and the structural failure mode. Moreover, under the (1 1 1)[$1 1 -2$] pure shear strains, the length of the N-Ti₁ (and the equivalent N-Ti₂, N-Ti₄, and N-Ti₅) bonds increases steadily from 2.13 Å to 2.52 Å; meanwhile, the length of the N-Ti₃ (and the equivalent) bonds contracts from 2.13 Å to 1.91 Å. Of the six N-Ti bonds, two-thirds are main load bearers that undergo considerable stretching. Meanwhile, under the pure shear strains along the (1 1 1)[$-1 -1 2$] or (1 1 1)[$-1 0 1$] directions, only one-third of the N-Ti bonds similarly bear the major load. The larger number of the main load-bearing bonds under the (1 1 1)[$1 1 -2$] pure shear strains produces a steeper rise of the stress, especially at larger strains, compared to the stress responses under the (1 1 1)[$-1 0 1$] and (1 1 1)[$-1 -1 2$] pure shear strains, which share the same main loading-bearing bonds and similar deformation modes with similar peak shear stresses.

A distinct deformation mode under the (1 1 1)[$1 1 -2$] pure shear strains is a much larger angular change compared to the other two cases. The angle α between the two nearest N-Ti bonds [see Figs. 1(a) and 1(c) for the definition] hold steady with a slight increase under the (1 1 1)[$-1 -1 2$] and (1 1 1)[$-1 0 1$] pure shear strains, leaving the bond-length increase as the main structural deformation mode; meanwhile, under the (1 1 1)[$1 1 -2$] pure shear strains, α decreases considerably from 90° to about 70°, and this angular deformation provides an extra channel for accommodating a much larger strain range, over which the stress response sustained by the larger number of N-Ti bonds reaches the much higher level as shown in Fig. 1(b).

During the pure shear deformation in the (1 1 1) plane, the Ti-Ti distance also undergo evolution with rising strains as shown in Fig. 2(c). It is seen that a majority of the Ti-Ti distances remain little changes or slightly decreased, contributing to maintaining or strengthening the crystal structure, while one or two Ti-Ti distances increase markedly due to the distortion of the crystal structure. Overall, the stress response is mainly determined by the N-Ti bonds that are stronger due to their mixed covalent and metallic bonding nature stemming from the native charge configurations of the constituent N and Ti atoms and their close spatial proximity that promote short and strong bonds.

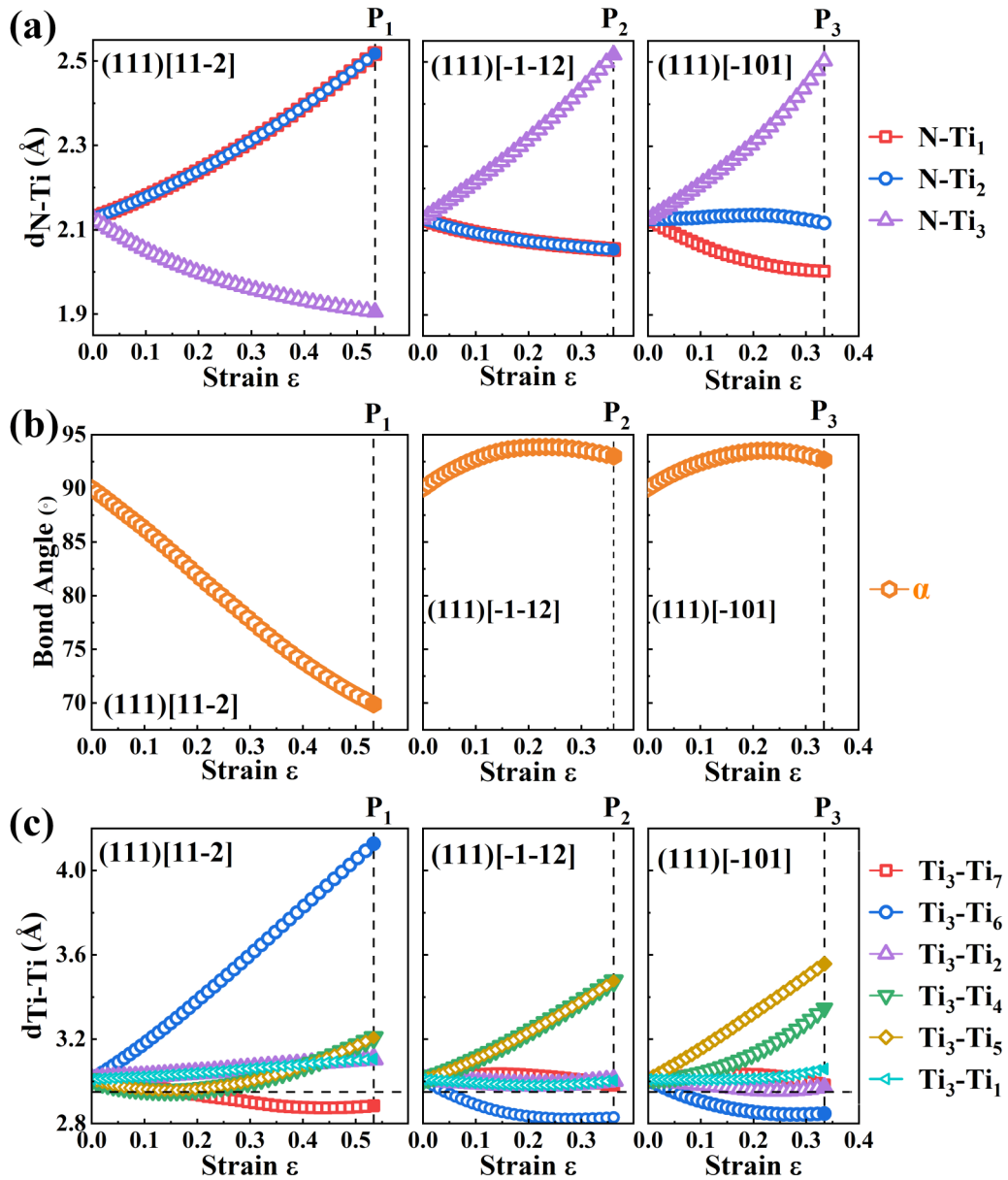


FIG. 2. The evolution of (a) the N-Ti bond length, (b) the Ti-N-Ti bond angle, and (c) the Ti-Ti distance under the indicated pure shear strains up to the point right before the large stress drop shown in Fig. 1(b). The subscripts label distinct Ti atoms surrounding a N atom as shown in Fig. 1(a). The horizontal-dashed lines in (c) mark the bond length of the Ti-Ti bonding in Ti metal at equilibrium [43].

B. Structural deformation and stress responses of TiN under indentation shear strains

Under the hardness testing conditions, an additional normal stress from the indenter is present conforming to the constraint imposed by the sharp slanted geometry of the indenter head, and this normal-stress component needs to be concurrently included in the simulation to properly account for its effect on the shear stress response of the tested specimen, which is crucial to determining its indentation strength and hardness. Here, we employ a computational approach [55,56] that incorporates the normal and shear stress components under an indenter with a specific centerline-to-face angle θ as described above in the Computational Methods section (Sec. II). For the Vickers and Berkovich indenters

that we examine in this paper, this angle takes the values of $\theta = 68.0$ and 65.3 degrees, respectively. Given that these two angles are close to each other, it is expected that the stress responses under the Vickers and Berkovich indentation are going to be similar. Our calculations generally support this expectation, but the results also reveal subtle yet substantive distinctions among the two sets of stresses. The ideal indentation shear strength, defined as the lowest peak stress under the indentation shear loadings, sets the theoretical limit that correlates closely with the intrinsic load-independent hardness. This approach has been demonstrated to provide a reliable description for a large number and variety of strong solids, including many TMLE compounds [24–29], in assessing their mechanical strength and hardness under various loading

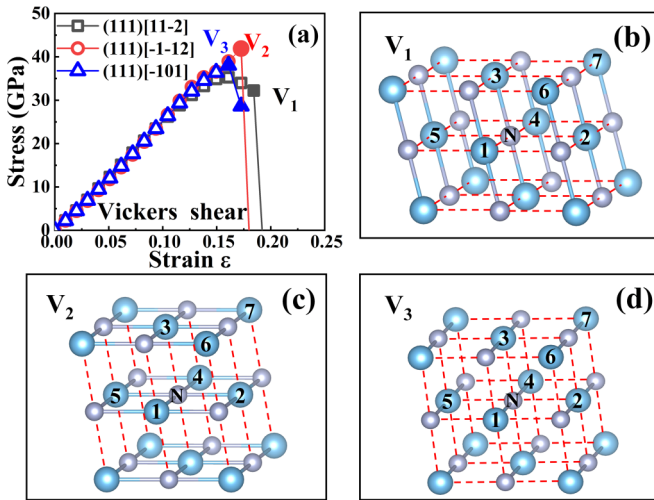


FIG. 3. (a) Calculated stress responses of TiN under Vickers shear strains in the $(1\ 1\ 1)$ plane along the high-symmetry $[1\ 1\ -2]$, $[-1\ -1\ 2]$ and $[-1\ 0\ 1]$ shear slip directions. [(b)–(d)] The corresponding structural snapshots right before the large drop of stress on the Vickers shear stress-strain curve. The dashed lines indicate the most stretched main load-bearing N-Ti bonds [see Fig. 4(a) for details].

conditions and unveiling the underlying atomistic deformation mechanisms, which are essential for elucidating fundamental materials physics and guiding rational material design and optimization tailored for diverse applications.

We show in Fig. 3(a) calculated stress responses of TiN under Vickers shear strains in the $(1\ 1\ 1)$ plane, which reveal surprising indentation (normal stress) modified shear stresses with significant changes in both the peak strain and stress values compared to those under the corresponding pure shear strains. First, there is a large suppression of the highest pure-shear stress peak along the $(1\ 1\ 1)[1\ 1\ -2]$ shear slip direction from 48.1 GPa under pure shear to 35.3 GPa under Vickers indentation and, remarkably, there is a concurrent substantial enhancement of the lower pure-shear stress peaks under the $(1\ 1\ 1)[-1\ -1\ 2]$ and $(1\ 1\ 1)[-1\ 0\ 1]$ shear slip directions from the original 28.7 GPa and 32.1 GPa under pure shear to 41.9 GPa and 38.0 GPa, respectively, under Vickers indentation. These rising lower peak stresses raise the ideal indentation shear strength and, together with the reduced higher peak stress, make the shear stress responses in the TiN $(1\ 1\ 1)$ plane from highly anisotropic under pure shear strains to nearly isotropic under the indentation strains. Another notable change in the stress responses induced by the indentation loading is a marked structural stiffening with a much higher rate of stress increase with the rising strain and a sharp stress drop shortly after reaching the peak value around 0.16, which is much reduced compared to the peak strains under the pure shear modes. This indentation modified stress behavior is typical of strong covalent crystals like diamond and cubic boron nitride [37], which is in sharp contrast to the pure shear case that hosts more moderate rise of the stress and the presence of a wide-plateau region with very slow rising of stresses approaching and past the shear stress peaks, as seen in Fig. 1(b). The behaviors of slow-changing stresses are reminiscent to those seen in metallic

materials [41], featuring smoother stress variations and larger deformation ranges. We also examined the stress response of TiN $(1\ 1\ 1)$ under Berkovich shear strains, and the results (see Fig. S1 in the Supplemental Material [67]) are almost the same as those under the Vickers shear strain, both showing a steep increase and abrupt drop after the peak value, and there are only slight differences in the peak stress values. Such similarities are expected due to the very close geometry of the Vickers and Berkovich indenters. These results indicate high intrinsic strength and hardness of well crystallized TiN $(1\ 1\ 1)$ specimens.

We show in Figs. 3(b)–3(d) the structural snapshots of deformed TiN crystal structure at the largest strains in the indicated shear slip directions right before their structural failure indicated by the abrupt steep drop of stress. These snapshots provide direct visual evidence for showcasing the structural response to the applied loading conditions as reflected by the bonding patterns in the severely strained crystal. It is seen that these strained bonding structures adopt similar deformation patterns under all three examined Vickers shear strains, which is in sharp contrast to the situation under pure shear strains [Fig. 1(c)] where bond elongations occur in the $(0\ 0\ 1)$ plane under the $(1\ 1\ 1)[1\ 1\ -2]$ shear strains but align perpendicular to the $(0\ 0\ 1)$ plane under the $(1\ 1\ 1)[-1\ -1\ 2]$ and $(1\ 1\ 1)[-1\ 0\ 1]$ shear strains. Under the indentation loading conditions, the extra normal stress under the indenter constrains the bond stretching in the $[0\ 0\ 1]$ direction, suppressing the tendency of the $(0\ 0\ 1)$ cleavage of the TiN crystal under the $(1\ 1\ 1)[-1\ -1\ 2]$ and $(1\ 1\ 1)[-1\ 0\ 1]$ shear strains and generating similar bonding patterns and Vickers indentation shear stress responses in all three examined slip directions as shown in Fig. 3(a). This loading dependent bond deformation process is responsible for the transition from the highly anisotropic stress responses under the pure shear strains to the largely isotropic stress responses under the indentation shear strains in the $(1\ 1\ 1)$ plane of TiN, and such behavior is expected to hold valid for more general material configurations based on the general underlying atomistic mechanisms.

To understand the nearly isotropic indentation stress responses in the $(1\ 1\ 1)$ plane in contrast to the more directional stress-strain relations under the corresponding pure shear strains, we analyze the evolution of the N-Ti bonds and Ti-Ti distances under the Vickers indentation strains. The results (Fig. 4) show that, compared with the structural changes under pure shear strains [Figs. 2(a) and 2(c)], the elongation of the main load-bearing bonds is suppressed by indentation induced normal compression in the $[0\ 0\ 1]$ direction, and the overall bond stretching is notably reduced. For example, the N-Ti3 bond length stretches to 2.50 Å under the pure shear strain in the $(1\ 1\ 1)[-1\ 0\ 1]$ direction, but this value is 2.27 Å under the Vickers indentation. Meanwhile, the normal stress also compresses the distance between selected Ti atoms to smaller than the Ti-Ti bond length of 2.95 Å in Ti metal [Fig. 4(b)]. In particular, under the $(1\ 1\ 1)[-1\ -1\ 2]$ Vickers shear, half of the neighboring Ti-Ti distances are shorter than 2.95 Å, which helps to enhance the strength. Under the $(1\ 1\ 1)[-1\ 0\ 1]$ Vickers indentation, the number of elongated N-Ti bonds doubles, leading to strengthening compared with the pure shear case. Consequently, indentation strengthens the two weaker directions under pure shear strains. On the

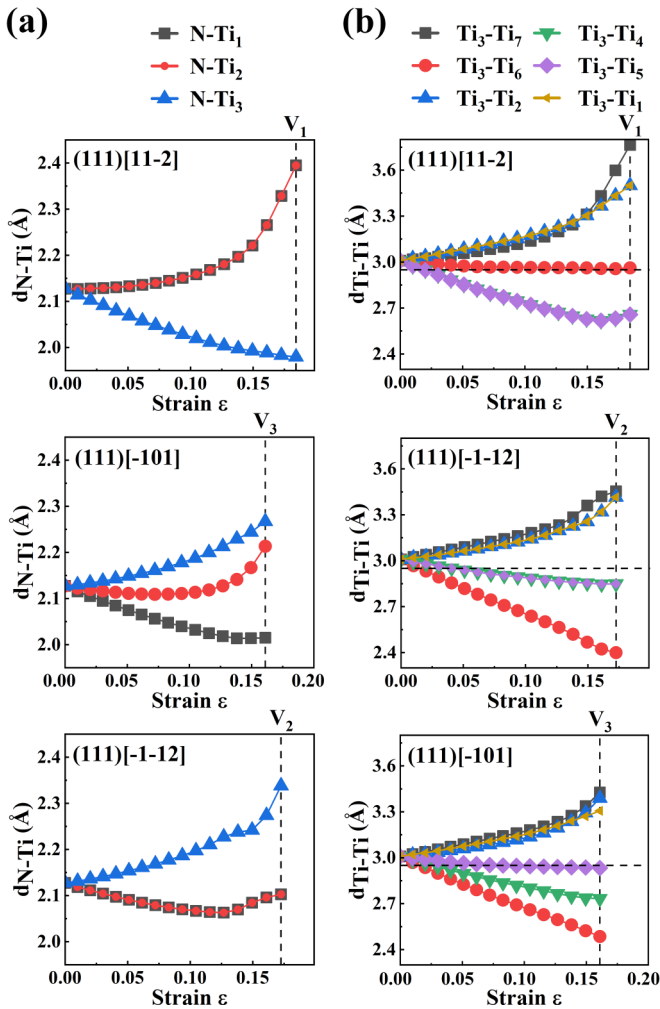


FIG. 4. The evolution of (a) N-Ti bond length and (b) Ti-Ti distance under the Vickers shear strains in the (1 1 1) plane along the indicated high-symmetry shear slip directions.

other hand, the stronger pure shear direction (1 1 1)[1 1 -2] maintains two N-Ti load-bearing bonds that are lengthened under indentation, but these bonds undergo large increases at much reduced strains, generating smaller stresses prior to the onset of structural instability. These processes produce the more isotropic stresses in the (1 1 1) plane under indentation.

C. Structural deformation and stress responses of TiN under wear shear strains

Under many application conditions, there often exist flat-surface contact scenarios, where a nearly constant normal-stress constraints shear loadings, as in the omnipresent cases of wear and frictional contacts. To probe such mechanical setups and associated processes, we have performed stress-strain calculations and analyzed the shear stress responses in the presence of a constant normal stress over a wide range up to 40 GPa to obtain a systematic and in-depth understanding of normal-stress induced phenomena and the underlying mechanism. The calculated results (Fig. 5) unveil a systematic shear strength enhancement, which is more pronounced in the (1 1 1)[-1 -1 2] and (1 1 1)[-1 0 1] shear directions

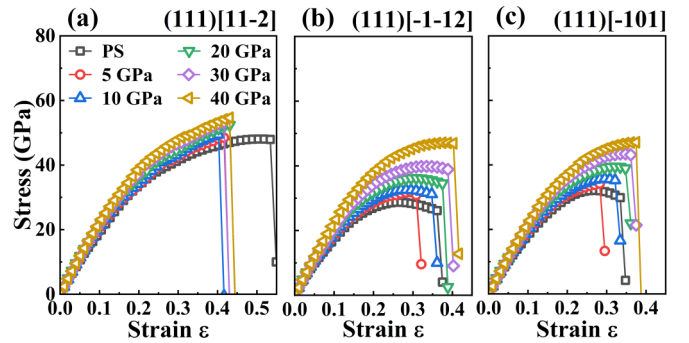


FIG. 5. The calculated stress responses of TiN under the constrained shear strains in the presence of different constant normal compressive stresses in the (1 1 1) plane along the high-symmetry (a) [1 1 -2], (b) [-1 -1 2], and (c) [-1 0 1] shear slip directions.

that host weaker pure shear strengths. As a result, the stress responses in various shear directions become more isotropic, approaching even exceeding 40 GPa, which is the threshold commonly designated for materials in the superhard category. This load induced strength enhancement is rare among TMLE compounds, including borides, carbides, and nitrides, which tend to soften when a normal load is introduced into shear deformation process [24–26]. This special mechanical character highlights exceptional suitability of TiN as a superior material that reacts favorably to practical loading conditions that commonly comprise both a shear and a normal stress component. In addition, the increases of both the peak stress and strain values, especially under the weaker pure shear cases, enhance the toughness of the material. Our simulation results therefore explain the superior wear resistance of TiN and offer crucial insights into its intricate stress-strain relations under broad practical loading conditions. We now examine the deformation and bonding changes under various constrained shear strains to elucidate the atomistic mechanisms for remarkable strain strengthening in TiN, which has a cubic crystal symmetry that was considered unfavorable for sustaining large deformation under concurrent normal and shear strains [36]. Here, we first analyze the variation of bond length during the strain process under different constant normal compressive stress along the originally weakest (1 1 1)[-1 -1 2] shear direction, as shown in Fig. 6. As the constant normal stress increases, the N-Ti bonds remain largely unaffected, while the Ti-Ti distance is more sensitive to the changing normal stress and undergoes divergent changes, with some becoming longer while other shorter, differently impacting stress responses. Specifically, the Ti-Ti distance in the [1 1 0] direction decreases significantly, notably enhancing the (1 1 1)[-1 -1 2] shear strength. Meanwhile, the (1 1 1)[-1 0 1] shear strength is similarly enhanced via similar bond-length variations patterns (see Fig. S2 in the Supplemental Material [67]). However, in the (1 1 1)[1 1 -2] direction, the change of Ti-Ti distance is smaller under rising normal stress (see Fig. S3 in the Supplemental Material [67]), resulting in smaller shear strength increase. These results highlight the delicate direction-sensitive bonding variations in response to normal-stress constrained shear deformation modes that are commonly encountered in friction and wear processes,

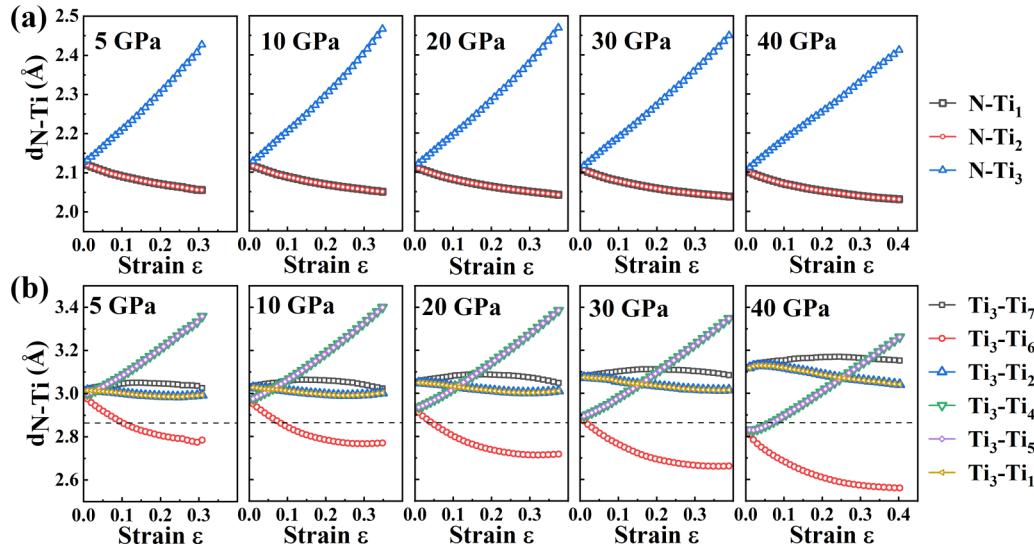


FIG. 6. The evolution of (a) the N-Ti bond lengths and (b) the Ti-Ti distances under the constrained shear strains in the presence of different constant normal compressive stress in the (1 1 1) plane along the $[-1 -1 2]$ shear slip direction.

which could involve loading conditions with very high normal stresses.

D. Loading dependent brittle-ductile behaviors of TiN under versatile shear strains

The indentation induced changes in structural deformation modes produce large strain stiffening that raises the lower peak shear stresses and consequently leads to higher indentation strength and hardness; in the meantime, the indentation constrained deformation modes also make the crystal more brittle as indicated by the considerably reduced peak shear strain and the abrupt loss of strength past the peak stress [Fig. 3(a)]. Such behaviors are commonly seen in brittle solids in which bonds can sustain only relatively small strains without much ability to sustain elongation beyond the peak stress [37]. A quantitative measure of ductile/brittle nature of a material can be obtained by integrating its stress response curve along a specific deformation path up to the strain of the sharp stress drop that indicates the onset of incipient plasticity, which gives the material's ability of sustaining structural deformation without catastrophic failure [68]. For TiN, the integration of the pure-shear stress curve under the (1 1 1) $[-1 -1 2]$ pure shear mode to the bond-breaking strain of 0.36 gives a value of 7.76, which is much higher than the values of 3.67 and 3.18 under the corresponding Vickers indentation shear strains. These results show that the indentation process greatly enhances the brittleness of TiN compared to its more ductile nature under the pure shear strains.

This intriguing issue is further examined below under the wear shear strains, which is a typical loading condition with a distinct normal-to-shear relation often experienced in wide-ranging equipment and device applications where significant wear and friction is generated with (kinetic) or without (static) the relative sliding motion at the contact surface. As shown in Fig. 7, the integrated area of the shear stress response curves under constant normal constrained shear along all the examined direction in the (1 1 1) plane first decrease at relatively low

constant normal compression and then increase. For the (1 1 1) $[1 1 -2]$ direction, the transition point is around 10 GPa; meanwhile, for the other two directions, the transition point is around 5 GPa and the results rise much higher than the pure-shear values. It is noted that the integrated areas under the shear stress response curves under normal stresses are all significantly larger than those under the corresponding Vickers or Berkovich indentation shear deformation. These results reveal considerable normal-stress induced changes in the ductility and toughness of TiN.

The pronounced change of the ductile-brittle characters of TiN under different strain conditions raises a fundamental issue regarding the description of material behaviors that depend sensitively on the loading conditions. In particular, the traditional methods of characterizing the material properties like strength and hardness may need further in-depth analysis

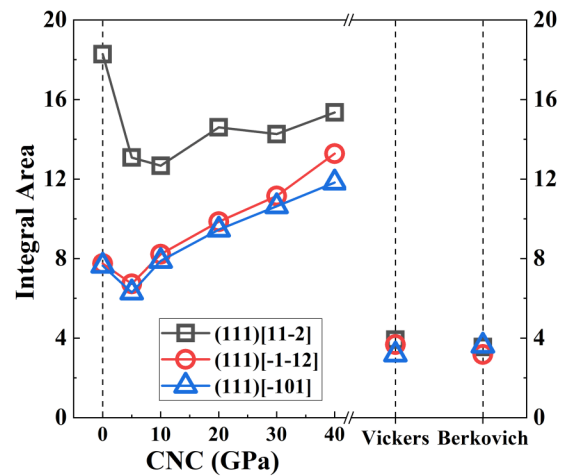


FIG. 7. The integrated area of the stress response curves along the indicated shear strains under various constant normal compressive (CNC) stress. The results for corresponding Vickers and Berkovich shear deformation cases are also shown for comparison.

to properly account for their rich behaviors revealed in this paper. The hardness-testing based evaluation may drive the material into structural and bonding-state transitions toward the more brittle nature, as exemplified here in the case of TiN, which is expected to be more generally applicable in a broad range of TMLE compounds that possess similar bonding environments. Meanwhile, the same material may exhibit much more ductile and tough mechanical characteristics under different loading conditions, such as those encountered in the friction and wear environments. This intriguing phenomenon should be taken into consideration when design and analyze material behaviors for applications where the loading conditions similar or distinct compared to those encountered during the testing procedures may arise and cause very different behaviors in the nature of key material performance characteristics. In particular, an indentation test determined brittle material may behave notably more ductile under other (e.g., friction and wear) loading conditions.

It is noted that although the integral area of the shear stress-strain curve with the stress drop provides a useful indication of the brittle-ductile change in the elastic region, the results are approximate. This phenomenon may be more complex and requires further consideration of other processes such as dislocation nucleation, crack propagation, etc. [69–71], which were not treated in the preset paper.

It should be mentioned that cleavage failure is also a possibility. If the strain energy of breaking bonds in shear is very large compared to the energy involved in bond breaking in tension, it will be kinetically easier to relax the stored elastic energy by cleavage [68]. For example, the critical cleavage stress of TiN along the $\langle 111 \rangle$ direction is 27 GPa [72], which is less than our calculated critical shear stress, and tension induced structural failure may occur under proper loading conditions.

E. Crystal-orientation dependent mechanical strength and hardness of TiN

Traditional description of hardness gives a single aggregate value, but mechanical properties are expected to be sensitive to crystal orientations hosting distinct bonding structures. To gain insights, we explore stress responses in the (110) and (100) planes of TiN, in addition to the results in the (111) plane examined above. We show in Fig. 8 calculated results under pure shear and Vickers shear strains. Results under Berkovich shear strains are similar to those under Vickers shear strains (see Fig. S4 in the Supplemental Material [67]). The pure shear stresses in the (110) plane are highly anisotropic. The highest peak stress occurs in the $(110)[\bar{1}\bar{1}2]$ direction with a value of 55.8 GPa, while the $(110)[1\bar{1}0]$ and $(110)[1\bar{1}1]$ directions exhibit weaker stress responses, with the peak stresses of 29.0 GPa and 32.0 GPa, respectively. In contrast, the results in the (100) plane are nearly isotropic, with the peak shear stresses in the $[001]$, $[011]$, and $[012]$ directions being 36.2 GPa, 33.0 GPa, and 33.9 GPa, respectively. Similar to the case of the (111) plane shown in Fig. 1, these orientation dependent stress behaviors are rooted in distinct deformation modes as illustrated by the snapshots at the strains before the sharp stress drop (see Fig. S5 in the Supplemental Material [67]).

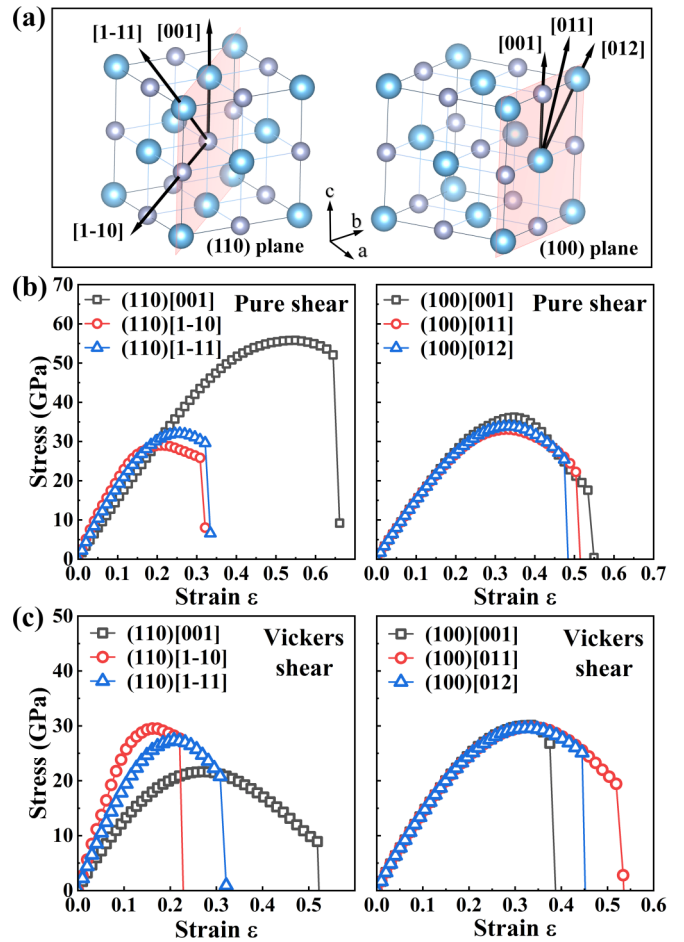


FIG. 8. (a) A schematic view of the high symmetry directions in the (110) and (001) planes. The calculated stress responses of TiN under (b) the indicated pure shear strains and (c) the corresponding Vickers shear strains in the (110) and (001) planes along the selected high-symmetry shear slip directions.

Under Vickers shear strains, the stress responses in the (110) plane undergo drastic changes. The strongest pure shear $[001]$ direction becomes the weakest direction, with the peak shear stress dropping to 21.6 GPa, while the peak shear stresses in the $[1\bar{1}0]$ and $[1\bar{1}1]$ directions become 29.5 GPa and 27.4 GPa, respectively. Meanwhile, the shear stress responses in the (100) plane turn highly isotropic, with the peak Vickers shear stresses in the $[001]$, $[011]$, and $[012]$ directions being 30.1 GPa, 29.8 GPa, and 29.6 GPa, respectively. The evolution of N-Ti bonds underlying these stress behaviors are given in Fig. S6 (see the Supplemental Material [67]). It is known that the lowest peak stress sets the threshold stress at which a perfect crystal becomes mechanically unstable [55,56]. Based on this criterion, the Vickers indentation strengths of TiN rank in the order of $(111) > (100) > (110)$, which is the same as the order of the experimentally measured hardness values [63], whereas the corresponding pure shear strengths (i.e., the lowest pure shear peak stresses) give a different rank of $(100) > (110) > (111)$. These results indicate that indentation strength offers a more accurate description than pure shear strength, with the former

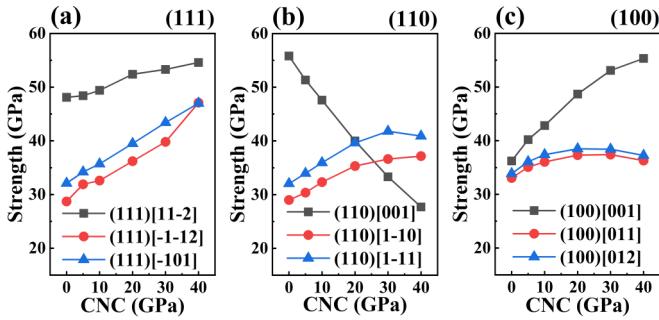


FIG. 9. Shear strengths of TiN under different constant normal compression (CNC) in the (a) (1 1 1), (b) (1 1 0), and (c) (1 0 0) plane along the indicated high-symmetry shear slip directions (pertinent full stress-strain curves are given in the Supplemental Material Fig. S7 [67]).

capturing key bonding and stress responses under the hardness testing loading conditions.

We have checked the stress responses under shear strains under constant normal compression constraints. Figure 9 shows the shear strengths (i.e., the lowest peak stress) in the (1 1 1), (1 1 0), and (1 0 0) planes of TiN under various constant normal compression, which reflect distinct load-bearing bonding patterns and stress responses related to the changing crystal orientations and loading conditions. The bonding changes underlying the large strength reduction under the (1 1 0)[0 0 1] shear strains are given in Fig. S8 (see the Supplemental Material [67]).

Our study shows that the structural deformation modes and stress responses of TiN sensitively dependent on crystal orientation, leading to distinct mechanical properties like strength and hardness with widely varying magnitudes, trends and mechanisms. These findings offer a more comprehensive and in-depth description of material behaviors at large strains up to the elastic limits on distinct crystal planes, thereby going beyond traditional characterization methods that use the elastic parameters at the equilibrium structure or adopt such parameters as input into empirical formulas to generate a single hardness value for a given material. The present results offer an explanation for the commonly observed scattering of measured hardness results, caused by orientation dependent variations, in addition to other factors like load, loading rate, surface condition, etc. These insights enable a better understanding of experimental phenomena and further design and optimization of materials with enhanced properties.

IV. CONCLUSIONS

In this paper, we take TiN as an exemplary case study among the vast TMLE compounds for an in-depth evaluation of structural and mechanical properties in a wide variety and range of deformation modes that are often encountered in practical loading conditions. We aim to identify desirable

but uncommon phenomena of strain induced strengthening and effective tuning of mechanical properties to help understand fundamental material behaviors and guide performance optimization. Extensive first-principles calculations of stress-strain relations unveil distinct atomistic deformation mechanisms that produce stress responses showing sensitive dependence on crystal orientation and loading conditions. These findings establish fundamental understanding of intrinsically diverse nature of mechanical properties in crystals exhibiting directional bonding characters that are present in many technologically important materials. The results reported here offer insights for elucidation of experimental observations and rational optimization of mechanical properties of TiN, and the knowledge gained from this study holds promise for further identification and development of materials among the large class of TMLE compounds that possess superior mechanical properties via computationally guided material design and discovery.

Recent studies have shown that normal-stress constrained shear deformation can produce unprecedented structural, mechanical, and electronic properties in strongly covalent solids like diamond, silicon, and silicon carbide, leading to unusual and robust metallic and superconducting states [73–75] in these quintessential semiconductors. In the present paper, we show that under normal-stress constraints, a rich variety of shear deformation modes can occur, resulting in significant strengthening and tuning of the mechanical properties of TiN that comprises mixed covalent and metallic bonding characters, thus extending the effective and versatile strain tuning of key material properties to a distinct and broad class of materials with both fundamental and practical significance. The mechanisms unveiled here are expected to drive similar phenomena in transition-metal nitrides, borides, and carbides that share many of the same structural and bonding characters. The prominent and robust material response characteristics such as orientation dependent strength and hardness variation, load sensitive brittle-ductile change, and normal-stress induced stress isotropy highlight a rich variety of mechanical benchmarks that can be tapped for property modulation and performance optimization, thereby opening new possibilities for tuning TMLE compounds for wide-ranging applications under diverse loading conditions.

ACKNOWLEDGMENTS

This work was supported by the National Natural Science Foundation of China (Grants No. 51972139 and No. 51602122), the China Postdoctoral Science Foundation (Grant No. 2020M681031), and the Science and Technology Development Program of Jilin province (Grant No. 20210101062JC). The reported calculations utilized computing facilities at the High-Performance Computing Center of Jilin University.

[1] V. V. Brazhkin, A. G. Lyapin, and R. J. Hemley, *Philos. Mag. A* **82**, 231 (2002).

[2] E. Gregoryanz, C. Sanloup, M. Somayazulu, J. Badro, G. Fiquet, H.-K. Mao, and R. J. Hemley, *Nat. Mater.* **3**, 294 (2004).

- [3] R. B. Kaner, J. J. Gilman, and S. H. Tolbert, *Science* **308**, 1268 (2005).
- [4] R. W. Cumberland, M. B. Weinberger, J. J. Gilman, S. M. Clark, S. H. Tolbert, and R. B. Kaner, *J. Am. Chem. Soc.* **127**, 7264 (2005).
- [5] J. C. Crowhurst, A. F. Goncharov, B. Sadigh, C. L. Evans, P. G. Morrall, J. L. Ferreira, and A. Nelson, *Science* **311**, 1275 (2006).
- [6] A. F. Young, C. Sanloup, E. Gregoryanz, S. Scandolo, R. J. Hemley, and H.-k. Mao, *Phys. Rev. Lett.* **96**, 155501 (2006).
- [7] H.-Y. Chung, M. B. Weinberger, J. B. Levine, A. Kavner, J.-M. Yang, S. H. Tolbert, and R. B. Kaner, *Science* **316**, 436 (2007).
- [8] J. B. Levine, S. L. Nguyen, H. I. Rasool, J. A. Wright, S. E. Brown, and R. B. Kaner, *J. Am. Chem. Soc.* **130**, 16953 (2008).
- [9] Q. Gu, G. Krauss, and W. Steurer, *Adv. Mater.* **20**, 3620 (2008).
- [10] J. Qin, D. He, J. Wang, L. Fang, L. Lei, Y. Li, J. Hu, Z. Kou, and Y. Bi, *Adv. Mater.* **20**, 4780 (2008).
- [11] A. Friedrich, B. Winkler, L. Bayarjargal, W. Morgenroth, E. A. Juarez-Arellano, V. Milman, K. Refson, M. Kunz, and K. Chen, *Phys. Rev. Lett.* **105**, 085504 (2010).
- [12] R. Mohammadi, A. T. Lech, M. Xie, B. E. Weaver, M. T. Yeung, S. H. Tolbert, and R. B. Kaner, *Proc. Natl. Acad. Sci. U.S.A.* **108**, 10958 (2011).
- [13] M. Xie, R. Mohammadi, Z. Mao, M. M. Armentrout, A. Kavner, R. B. Kaner, and S. H. Tolbert, *Phys. Rev. B* **85**, 064118 (2012).
- [14] X. Cheng, W. Zhang, X.-Q. Chen, H. Niu, P. Liu, K. Du, G. Liu, D. Li, H.-M. Cheng, H. Ye *et al.*, *Appl. Phys. Lett.* **103**, 171903 (2013).
- [15] M. Wang, Y. Li, T. Cui, Y. Ma, and G. Zou, *Appl. Phys. Lett.* **93**, 101905 (2008).
- [16] Q. Tao, D. Zheng, X. Zhao, Y. Chen, Q. Li, Q. Li, C. Wang, T. Cui, Y. Ma, X. Wang *et al.*, *Chem. Mater.* **26**, 5297 (2014).
- [17] M. Xie, R. Mohammadi, C. L. Turner, R. B. Kaner, A. Kavner, and S. H. Tolbert, *Phys. Rev. B* **90**, 104104 (2014).
- [18] H. Niu, J. Wang, X.-Q. Chen, D. Li, Y. Li, P. Lazar, R. Podlucky, and A. N. Kolmogorov, *Phys. Rev. B* **85**, 144116 (2012).
- [19] H. Gou, N. Dubrovinskaia, E. Bykova, A. A. Tsirlin, D. Kasinathan, W. Schnelle, A. Richter, M. Merlini, M. Hanfland, A. M. Abakumov, D. Batuk, G. Van Tendeloo, Y. Nakajima, A. N. Kolmogorov, and L. Dubrovinsky, *Phys. Rev. Lett.* **111**, 157002 (2013).
- [20] A. Knappschneider, C. Litterscheid, D. Dzivenko, J. A. Kurzman, R. Seshadri, N. Wagner, J. Beck, R. Riedel, and B. Albert, *Inorg. Chem.* **52**, 540 (2013).
- [21] Q. Wang, J. He, W. Hu, Z. Zhao, C. Zhang, K. Luo, Y. Lü, C. Hao, W. Lü, Z. Liu *et al.*, *J. Mater. Chem. A* **1**, 45 (2015).
- [22] C. Brookes and E. Brookes, *Diamond Relat. Mater.* **1**, 13 (1991).
- [23] H. Sumiya and T. Irifune, *Diamond Relat. Mater.* **13**, 1771 (2004).
- [24] C. Zang, H. Sun, and C. Chen, *Phys. Rev. B* **86**, 180101(R) (2012).
- [25] C. Zang, H. Sun, J. S. Tse, and C. Chen, *Phys. Rev. B* **86**, 014108 (2012).
- [26] B. Li, H. Sun, C. Zang, and C. Chen, *Phys. Rev. B* **87**, 174106 (2013).
- [27] B. Li, H. Sun, and C. Chen, *Phys. Rev. B* **90**, 014106 (2014).
- [28] H. Wu, H. Sun, and C. Changfeng, *Appl. Phys. Lett.* **105**, 211901 (2014).
- [29] Q. Li, D. Zhou, W. Zheng, Y. Ma, and C. Chen, *Phys. Rev. Lett.* **115**, 185502 (2015).
- [30] C. Lu, W. Gong, Q. Li, and C. Chen, *J. Phys. Chem. Lett.* **11**, 9165 (2020).
- [31] Y. Tian, B. Xu, D. Yu, Y. Ma, Y. Wang, Y. Jiang, W. Hu, C. Tang, Y. Gao, K. Luo *et al.*, *Nature (London)* **493**, 385 (2013).
- [32] Q. Huang, D. Yu, B. Xu, W. Hu, Y. Ma, Y. Wang, Z. Zhao, B. Wen, J. He, Z. Liu *et al.*, *Nature (London)* **510**, 250 (2014).
- [33] B. Li, H. Sun, and C. Chen, *Nat. Commun.* **5**, 4965 (2014).
- [34] B. Li, H. Sun, and C. Chen, *Phys. Rev. Lett.* **117**, 116103 (2016).
- [35] S. Wang, X. Yu, Z. Lin, R. Zhang, D. He, J. Qin, J. Zhu, J. Han, L. Wang, H.-k. Mao *et al.*, *Chem. Mater.* **24**, 3023 (2012).
- [36] C. Lu, Q. Li, Y. Ma, and C. Chen, *Phys. Rev. Lett.* **119**, 115503 (2017).
- [37] Y. Zhang, H. Sun, and C. Chen, *Phys. Rev. B* **73**, 144115 (2006).
- [38] R. H. Telling, C. J. Pickard, M. C. Payne, and J. E. Field, *Phys. Rev. Lett.* **84**, 5160 (2000).
- [39] H. Chacham and L. Kleinman, *Phys. Rev. Lett.* **85**, 4904 (2000).
- [40] S.-H. Jhi, S. G. Louie, M. L. Cohen, and J. W. Morris, Jr., *Phys. Rev. Lett.* **87**, 075503 (2001).
- [41] S. Ogata, J. Li, and S. Yip, *Science* **298**, 807 (2002).
- [42] D. M. Clatterbuck, C. R. Krenn, M. L. Cohen, and J. W. Morris, Jr., *Phys. Rev. Lett.* **91**, 135501 (2003).
- [43] S. Ogata, J. Li, N. Hirotsuki, Y. Shibutani, and S. Yip, *Phys. Rev. B* **70**, 104104 (2004).
- [44] X. Blase, P. Gillet, A. San Miguel, and P. Mélinon, *Phys. Rev. Lett.* **92**, 215505 (2004).
- [45] Y. Zhang, H. Sun, and C. Chen, *Phys. Rev. Lett.* **93**, 195504 (2004).
- [46] Y. Zhang, H. Sun, and C. Chen, *Phys. Rev. Lett.* **94**, 145505 (2005).
- [47] M. G. Fyta, I. N. Remediakis, P. C. Kelires, and D. A. Papaconstantopoulos, *Phys. Rev. Lett.* **96**, 185503 (2006).
- [48] W. Gong, C. Liu, X. Song, Q. Li, Y. Ma, and C. Chen, *Phys. Rev. B* **100**, 220102(R) (2019).
- [49] C. Liu, X. Gu, K. Zhang, W. Zheng, Y. Ma, and C. Chen, *Phys. Rev. B* **105**, 024105 (2022).
- [50] X. Song, C. Liu, Q. Li, R. J. Hemley, Y. Ma, and C. Chen, *Proc. Natl. Acad. Sci. U.S.A.* **119**, e2122691119 (2022).
- [51] C. R. Krenn, D. Roundy, M. L. Cohen, D. C. Chrzan, and J. W. Morris, Jr., *Phys. Rev. B* **65**, 134111 (2002).
- [52] M. I. Eremets, I. A. Trojan, P. Gwaze, J. Huth, R. Boehler, and V. D. Blank, *Appl. Phys. Lett.* **87**, 141902 (2005).
- [53] T. Li, J. W. Morris, Jr., N. Nagasako, S. Kuramoto, and D. C. Chrzan, *Phys. Rev. Lett.* **98**, 105503 (2007).
- [54] A. Gouldstone, H.-J. Koh, K.-Y. Zeng, A. Giannakopoulos, and S. Suresh, *Acta Mater.* **48**, 2277 (2000).
- [55] Z. Pan, H. Sun, and C. Chen, *Phys. Rev. Lett.* **98**, 135505 (2007).
- [56] Z. Pan, H. Sun, Y. Zhang, and C. Chen, *Phys. Rev. Lett.* **102**, 055503 (2009).
- [57] G. Kresse and J. Furthmüller, *Phys. Rev. B* **54**, 11169 (1996).
- [58] G. Kresse and D. Joubert, *Phys. Rev. B* **59**, 1758 (1999).
- [59] J. P. Perdew, K. Burke, and M. Ernzerhof, *Phys. Rev. Lett.* **77**, 3865 (1996).
- [60] H. J. Monkhorst and J. D. Pack, *Phys. Rev. B* **13**, 5188 (1976).

- [61] P. Šajgalík, Z. Lenčič, and M. Hnatko, in *Ceramics Science and Technology: Vol. 2: Materials and Properties*, edited by R. Riedel and I-W. Chen (Wiley VCH, Weinheim, 2010), pp. 59–89.
- [62] Z. S. Rak and J. Czechowski, *J. Eur. Ceram. Soc.* **18**, 373 (1998).
- [63] H. Ljungcrantz, M. Odén, L. Hultman, J. Greene, and J.-E. Sundgren, *J. Appl. Phys.* **80**, 6725 (1996).
- [64] S.-Y. Chun, *J. Korean Phys. Soc.* **56**, 1134 (2010).
- [65] H. C. Barshilia, M. S. Prakash, D. S. Rao, and K. Rajam, *Surf. Coat. Technol.* **195**, 147 (2005).
- [66] Y.-W. Lin, H.-A. Chen, G.-P. Yu, and J.-H. Huang, *Thin Solid Films* **618**, 13 (2016).
- [67] See Supplemental Material at <http://link.aps.org/supplemental/10.1103/PhysRevB.106.054112> for more TiN stress-strain curves and the evolution of bond structure under various strains.
- [68] S. Ogata and J. Li, *J. Appl. Phys.* **106**, 113534 (2009).
- [69] J. R. Rice, *J. Mech. Phys. Solids* **40**, 239 (1992).
- [70] S. J. Zhou, A. E. Carlsson, and R. Thomson, *Phys. Rev. Lett.* **72**, 852 (1994).
- [71] P. Lazar and R. Podloucky, *Phys. Rev. B* **73**, 104114 (2006).
- [72] P. Lazar, J. Redinger, and R. Podloucky, *Phys. Rev. B* **76**, 174112 (2007).
- [73] C. Liu, X. Song, Q. Li, Y. Ma, and C. Chen, *Phys. Rev. Lett.* **123**, 195504 (2019).
- [74] C. Liu, X. Song, Q. Li, Y. Ma, and C. Chen, *Phys. Rev. Lett.* **124**, 147001 (2020).
- [75] C. Liu, X. Song, Q. Li, Y. Ma, and C. Chen, *Chin. Phys. Lett.* **38**, 086301 (2021).